Tespa1 negatively regulates FcεRI-mediated signaling and the mast cell–mediated allergic response

Di Wang,[1,2] Mingzhu Zheng,[1,2] Yuanjun Qiu,[1,2] Chuansheng Guo,[1,2] Jian Ji,[5] Lei Lei,[1,2] Xue Zhang,[2,3] Jingjing Liang,[1,2] Jun Lou,[1,2] Wei Huang,[1,2] Bowen Dong,[1,2] Songquan Wu,[6] Jianli Wang,[1] Yuehai Ke,[2,3] Xuetao Cao,[1,7] Yi Ting Zhou,[4] and Linrong Lu[1,2]

[1]Institute of Immunology, [2]Program in Molecular and Cellular Biology, [3]Department of Pathology and Pathophysiology, and [4]Department of Biochemistry and Molecular Biology, Zhejiang University School of Medicine, Hangzhou 310058, China
[5]Institute of Animal Science, Guangdong Academy of Agricultural Sciences, Guangzhou 510640, China
[6]Medical College of Lishui University, Lishui, Zhejiang 323000, China
[7]Institute of Immunology and National Key Laboratory of Medical Immunology, Second Military Medical University, Shanghai 200433, China

Antigen-mediated cross-linking of IgE on mast cells triggers a signaling cascade that results in their degranulation and proinflammatory cytokine production, which are key effectors in allergic reactions. We show that the activation of mast cells is negatively regulated by the newly identified adaptor protein Tespa1. Loss of Tespa1 in mouse mast cells led to hyper-responsiveness to stimulation via FcεRI. Mice lacking Tespa1 also displayed increased sensitivity to IgE-mediated allergic responses. The dysregulated signaling in KO mast cells was associated with increased activation of Grb2-PLC-γ1-SLP-76 signaling within the LAT1 (linker for activation of T cells family, member 1) signalosome versus the LAT2 signalosome. Collectively, these findings show that Tespa1 orchestrates mast cell activation by tuning the balance of LAT1 and LAT2 signalosome assembly.

CORRESPONDENCE
Di Wang:
diwang@zju.edu.cn
OR
Linrong Lu:
lu_linrong@zju.edu.cn

Abbreviations used: BALF, bronchoalveolar fluid; BMMC, BM-derived mast cell; FRET, fluorescence resonance energy transfer; LAT1, linker for activation of T cells family, member 1; PAS, periodic acid-Schiff; PCA, passive cutaneous anaphylaxis; PSA, passive systemic anaphylaxis.

Allergic responses are Th2- and IgE-mediated immune responses that evolved to protect against environmental substances and parasites. However, these responses can also lead to allergy when inadvertently activated by noninfectious environmental antigens and cause harmful symptoms such as itching, inflammation, or tissue injury. As to our current understanding, mast cells are at the center of allergic responses (Galli et al., 2005; Bischoff, 2007). Mast cells are BM-derived hematopoietic cells localized under surfaces exposed to the external environment, such as the skin, airways, and intestine. They function as sentinel cells in host defense reactions including immediate hypersensitivity responses and allergic responses (Galli et al., 2005). Activated mast cells trigger allergic responses by releasing preformed granule-associated chemical mediators, producing multiple cytokines and chemokines, and secreting de novo synthesized arachidonic acid metabolites and various proteins (Metcalfe et al., 1997; Bischoff, 2007).

Mast cells recognize antigens via IgE and specific Fc receptors, termed FcεRI. Binding of multivalent antigen to FcεRI-bound IgE induces receptor aggregation and triggers mast cell activation (Kinet, 1999; Siraganian, 2003). FcεRI is expressed on the surface of mast cell as a tetrameric complex consisting of an IgE-binding α subunit, a signal-modulating β subunit, and two signal-transduction γ subunits (Kraft and Kinet, 2007). The signaling cascades elicited by FcεRI aggregation in mast cells have been extensively studied (Kalesnikoff and Galli, 2008). Briefly, the conserved immunoreceptor tyrosine-based activation motifs (ITAMs) within the cytoplasmic tails of the β and γ subunits are rapidly phosphorylated upon FcεRI stimulation in a Lyn-dependent manner (Garman et al., 1999; Kinet, 1999). Then another tyrosine kinase, Syk, binds to the tyrosine-phosphorylated ITAMs

D. Wang and M. Zheng contributed equally to this work.

© 2014 Wang et al. This article is distributed under the terms of an Attribution–Noncommercial–Share Alike–No Mirror Sites license for the first six months after the publication date (see http://www.rupress.org/terms). After six months it is available under a Creative Commons License (Attribution–Noncommercial–Share Alike 3.0 Unported license, as described at http://creativecommons.org/licenses/by-nc-sa/3.0/).

The Rockefeller University Press $30.00
J. Exp. Med. 2014 Vol. 211 No. 13 2635–2649
www.jem.org/cgi/doi/10.1084/jem.20140470

The Journal of Experimental Medicine

and initiates the principal axis pathway that includes Grb2, PLC-γ1, and SLP-76 (Gilfillan and Tkaczyk, 2006; Rivera and Gilfillan, 2006), which ultimately lead to the activation of downstream signaling cascades including mitogen-activated protein kinases, protein kinase C pathways, and calcium flux.

During this signaling process, two similar adaptor proteins, linker for activation of T cells family, member 1 (LAT1) and LAT2, are both phosphorylated, resulting in the formation of two complementary and competitive signalosome complexes known as the LAT1 signalosome and the LAT2 signalosome. Both of these membrane adaptors recruit principal axis–related molecules including Grb2, SOS, PLC-γ1, SLP-76, and Vav1. The essential role of LAT1 in mast cell activation is clear because LAT1 deficiency markedly attenuates mast cell responsiveness. However, the function of the LAT2 signalosome in RcεRI signaling is still an enigma to many immunologists. In general, LAT2 may down-regulate antigen-mediated signaling in mast cells by either competing with LAT1 for a limited pool of signaling molecules or recruiting of phosphatases and ubiquitin-ligases such as SHP-1 and c-Cbl (Gu et al., 2001; Brdicka et al., 2002; Volná et al., 2004; Rivera, 2005). On the contrary, LAT2 has also been found to compensate for the loss of LAT1 in the *Lat1*$^{-/-}$ background (Volná et al., 2004; Zhu et al., 2004), either through activation of the principal axis pathway with lower efficiency, or by recruiting another adaptor protein, Gab2, to facilitate Fyn-Gab2-PI3K-Akt signaling termed the complementary axis (Gilfillan and Tkaczyk, 2006; Kalesnikoff and Galli, 2008; Alvarez-Errico et al., 2009).

The current model of LAT1 and LAT2 activation raises another unavoidable question of what determines the recruitment of the same pool of signaling molecules to two different adaptor proteins, namely LAT1 and LAT2, with such high similarity in sequence and structure. It is still unclear whether there is a shunt to modulate the allocation of the signal molecules to these different signalosomes. If such a regulator were found, it would be an attractive target for pharmacological intervention for fine-tuning allergic responses and the treatment of mast cell–driven disorders such as allergic asthma.

Recently, we identified a novel adaptor protein, Tespa1 (thymocyte-expressed, positive selection-associated 1), which plays a critical role in the positive selection of thymocytes (Wang et al., 2012). KO mice have fewer mature thymic CD4$^+$ and CD8$^+$ T cells due to impaired thymocyte development. We later demonstrated that Tespa1 associates with the TCR signaling components Grb2 and PLC-γ1, which in turn facilitates TCR signal transduction (Wang et al., 2012). Other than in T cells, *Tespa1* is also highly expressed in mast cells, as demonstrated by both real-time PCR analysis and the BioGPS gene expression atlas database (Su et al., 2004), suggesting a potential role of Tespa1 in mast cells.

To our great surprise, KO mast cells showed hyperresponsiveness to FcεRI stimulation, which is evidenced by enhanced cytokine production, degranulation, calcium mobilization, and elevated activation of downstream signaling pathways. Consistently, KO mice developed exacerbated anaphylactic response and allergic asthma. Our data revealed an unexpected function of Tespa1 as a negative regulator of FcεRI-mediated mast cell activation through fine-tuning of LAT1 and LAT2 signalosome assembling.

RESULTS

Expression of Tespa1 in mast cells and mast cell development in KO mice

Real-time PCR analysis showed that *Tespa1* mRNA expression was highly enriched in BM-derived mast cells (BMMCs), similar to its expression in CD4$^+$CD8$^+$ double-positive thymocytes, in contrast to its decreased expression levels in CD4$^+$ and CD8$^+$ single-positive thymocytes and low expression levels in BM-derived DCs and BM-derived macrophages (Fig. 1 a).

Our previous study has shown that Tespa1 deficiency did not affect the generation of BMMCs in the presence of IL-3 and stem cell factor. The yield and purity of mast cells cultured from Tespa1 WT and KO mice were comparable. The surface expression of FcεRI and c-Kit on KO BMMCs was identical to that on WT BMMCs (Wang et al., 2012). Moreover, the surface expression of two Toll-like receptor family

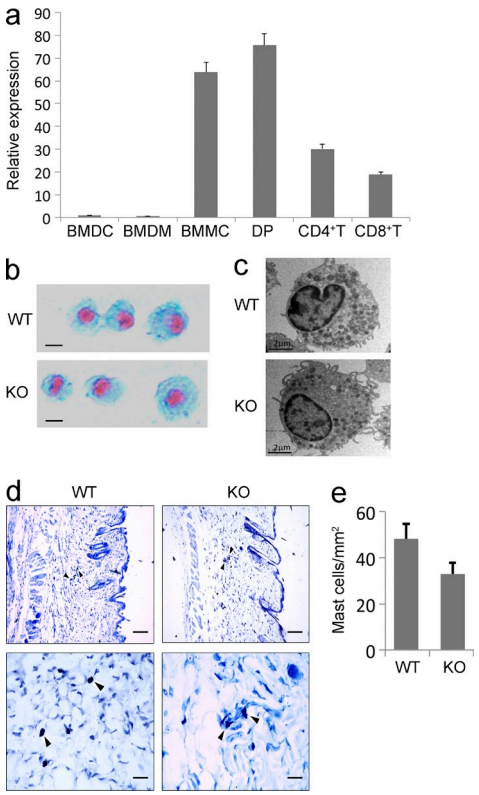

Figure 1. Tespa1 expression and BMMCs from WT and Tespa1-deficient mice. (a) *Tespa1* mRNA expression in various cell subsets was measured by RT-PCR. Results are presented relative to *Actb* expression. Error bars represent SD. (b) BMMCs were stained with Alcian blue-Safranin O. Bars, 2 µm. (c) BMMCs were analyzed by electron microscopy. Bars, 2 µm. (d) Tissue mast cells in skin sections were stained with toluidine blue. Arrowheads indicate mast cells stained with toluidine blue. Bars: (top row) 100 µm; (bottom row) 25 µm. (e) Absolute numbers of mast cells per mm^2 (mean and SD). Data are representative of three experiments.

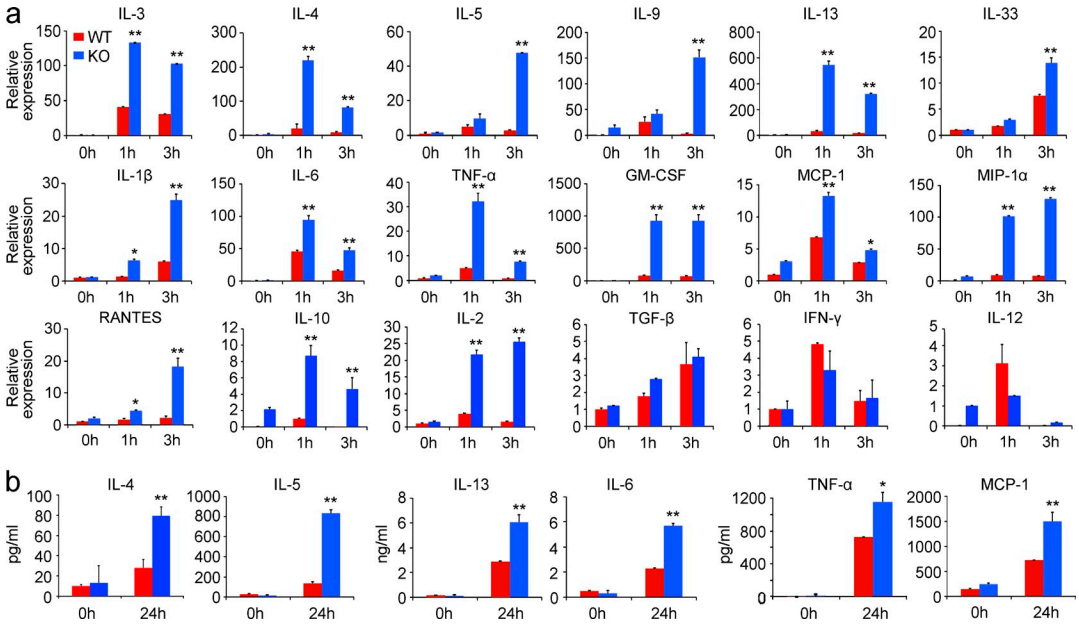

Figure 2. FcεRI-mediated cytokine and chemokine production by Tespa1-deficient mast cells. (a) WT and Tespa1 KO BMMCs were sensitized with anti-DNP IgE overnight and later stimulated with DNP-BSA for 1, 3, or 24 h. Cytokine and chemokine mRNA expression was measured by RT-PCR. (b) IL-4, IL-5, IL-13, IL-6, TNF, and MCP-1levels were measured by ELISA at 24 h. *, $P < 0.05$; **, $P < 0.01$ (Student's *t* test). Data are representative of three experiments. Error bars represent SD.

members, TLR2 and TLR4, were also unchanged in the Tespa1-deficient BMMCs (unpublished data). The KO mast cells did not differ morphologically from WT mast cells, as assessed by both Alcian blue–Safranin O staining and electron microscopy (Fig. 1, b and c). In vivo, the numbers of mast cells in back skin were not significantly altered in the KO mice compared with the WT controls when enumerated histologically after toluidine blue staining (Fig. 1, d and e).

Elevated FcεRI-mediated cytokine and chemokine production in KO mast cells

Engagement of the FcεRI receptor leads to the production of multiple cytokines and chemokines that play important roles in mast cell functions and allergic response. To determine whether Tespa1 is involved in the regulation of FcεRI-mediated cytokine and chemokine production, WT and KO BMMCs were sensitized with anti-DNP IgE and stimulated with DNP-BSA. Real-time PCR analysis showed dramatically and significantly increased expression of cytokine and chemokine mRNAs in the KO mast cells upon FcεRI aggregation. Those included Th2-related cytokines, inflammation-related cytokines, and chemokines. The production of immune regulation–related cytokines (including IL-10 and IL-2) was also significantly increased. However, the FcεRI-mediated production of TGF-β and Th1-related cytokines (including IFN-γ and IL-12) remained unaltered in the absence of Tespa1 (Fig. 2 a). Subsequent ELISA assay of the culture supernatant confirmed the significantly increased FcεRI-mediated secretion of IL-4, IL-5, IL-13, IL-6, TNF, and MCP-1 by KO mast cells (Fig. 2 b). We also profiled the FcεRI-mediated production of 15 mediators using Bio-Plex Suspension Array analysis and further confirmed the up-regulated production of these mediators in the absence of Tespa1 (unpublished data). Collectively, these data demonstrated that Tespa1 negatively regulates the cytokine and chemokine production in mast cells upon FcεRI aggregation.

Enhanced FcεRI-mediated degranulation and migration of KO mast cells

FcεRI-mediated BMMC activation also leads to rapid secretion of preformed inflammatory mediators such as histamine and arachidonic acid metabolites, referred to as degranulation (Metcalfe et al., 1997; Galli et al., 2008), which is also coupled with surface exposure of CD107a. We first found more pronounced up-regulation of CD107a cell surface expression in KO BMMCs upon FcεRI aggregation than in the WT control (Fig. 3 a). Next, we found that the release of histamine and leukotriene C4/D4/E4 was increased in KO BMMCs upon stimulation with suboptimal doses of allergen (Fig. 3, b and c).We further measured the release of β-hexosaminidase, a protein stored in preformed mast cell granules, and found that Tespa1 deficiency resulted in a substantial increase of allergen-elicited release of β-hexosaminidase from mast cells stimulated with DNP-BSA (Fig. 3 d). Degranulation is coupled with cytoskeletal rearrangement which can be monitored by xCELLigence, a microelectronic cell sensor-based technology (Abassi et al., 2004). BMMCs were cultured on the fibrinogen-coated surface of microelectronic cell sensor arrays integrated into the bottom of microtiter plates. The electrical properties reflect the impedance between cell membrane and

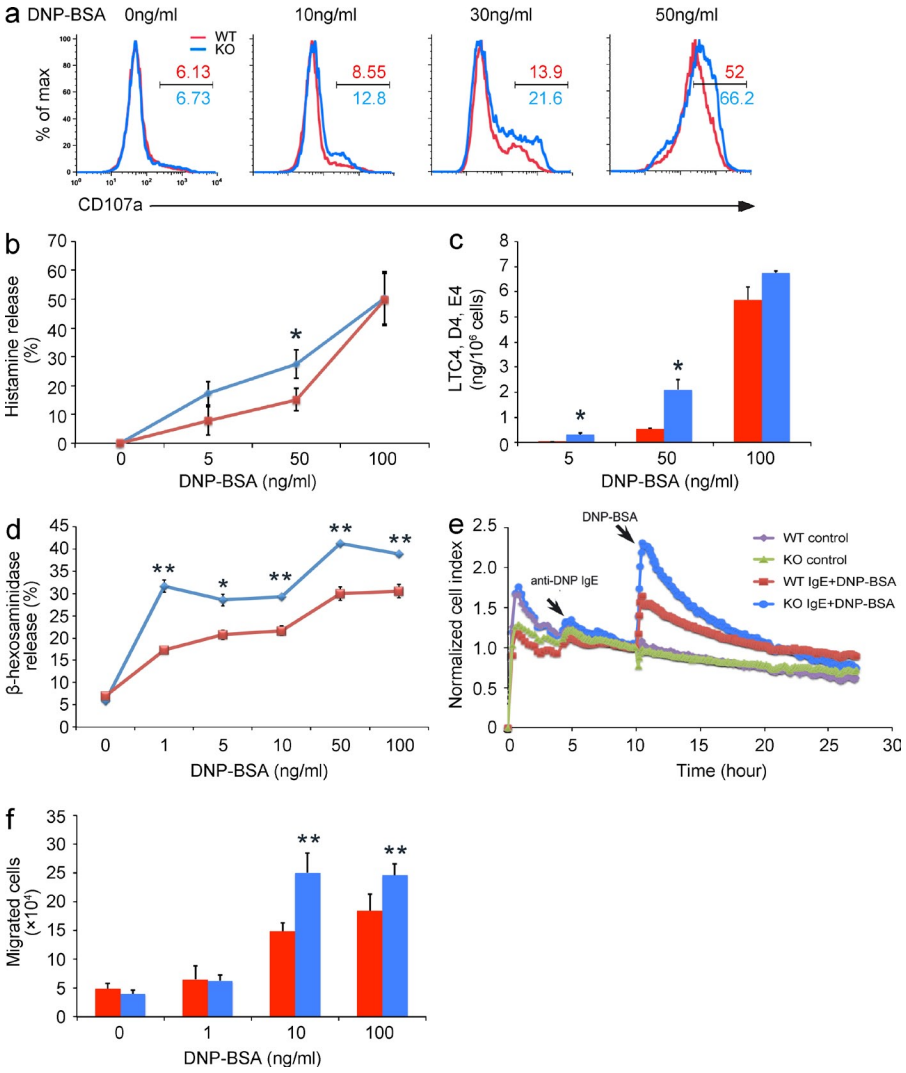

Figure 3. FcεRI-mediated degranulation and migration of Tespa1-deficient mast cells. (a) Tespa1 WT and KO BMMCs were sensitized with anti-DNP IgE overnight and stimulated with indicated concentrations of DNP-BSA for 10 min. Degranulation was assessed by CD107a levels. Numbers above and below bracketed lines indicated percentages of CD107a$^+$ cells. (b) Tespa1 WT and KO BMMCs were sensitized with anti-DNP IgE overnight and stimulated with indicated concentrations of DNP-BSA for 1 h. Degranulation was assessed by histamine release (presented as percentages of total histamine content). (c) BMMCs were stimulated as in b, and LTC4, D4, and E4 secretion was measured by competitive ELISA (Neogen). (d) BMMCs were stimulated with indicated concentrations of DNP-BSA for 30 min and degranulation was measured by β-hexosaminidase level. (e) Tespa1 WT and KO BMMCs were seeded onto the fibrinogen-coated surface of microelectronic cell sensor arrays integrated into the bottom of the microtiter plates, and the impedance was measured every 5 min and analyzed by xCelligence (real-time Cell Analyzer). (f) BMMCs were seeded on fibronectin-coated polycarbonate transwell filters, and anti-DNP IgE-sensitized BMMCs were loaded into the upper chamber. The lower chamber contained the indicated concentrations of DNP-BSA, and migrated cells were stained and counted after 6 h. *, $P < 0.05$; **, $P < 0.01$ (Student's *t* test). Data are representative of three experiments (mean and SD in b–d and f).

sensor surface. This represents the cytoskeletal changes during mast cell activation and was quantitatively and continuously recorded. We found that Tespa1 deficiency markedly increased the normalized cell index of BMMCs, which correlated well with enhanced degranulation (Abassi et al., 2004; Fig. 3 e). Migration is another cardinal feature of FcεRI-induced mast cell activation (Galli et al., 2005; Xiao et al., 2011). IgE-sensitized WT BMMCs were attracted toward the allergen, whereas this response was enhanced in KO BMMCs (Fig. 3 f). Together, these data indicated that Tespa1 negatively regulates FcεRI-mediated BMMC degranulation and migration.

Enhanced anaphylactic and allergic responses in KO mice

To evaluate the role of Tespa1 in mast cell activation in vivo, passive anaphylaxis was assessed in two models. The first model was passive systemic anaphylaxis (PSA), an IgE-mediated type I immediate hypersensitivity reaction. WT and KO mice were sensitized with anti-DNP IgE and then intravenously injected with DNP-BSA to elicit an anaphylactic response. Rectal temperature was recorded as a monitor of the magnitude of the PSA response. Neither WT nor KO mice injected with PBS showed any rectal temperature change. In contrast, mice challenged with DNP-BSA showed an evident rectal temperature drop by 20–25 min after injection, and a greater temperature drop occurred in KO mice than in WT mice (Fig. 4 a). Consistently, the anaphylactic response–elicited release of histamine and MCP-1 were significantly elevated in the serum of KO mice compared with the WT controls (Fig. 4 b).

The second model was passive cutaneous anaphylaxis (PCA) in the ear and back skin, which typically develops in the late phase (2–6 h) after allergen exposure. PCA was elicited by subcutaneous injection of anti-DNP IgE into the ear or back skin. After 24 h, mice received DNP-BSA together with Evans blue dye via intravenous injection. The ear swelling in KO mice was significantly greater than that in WT mice during most of the entire 22-h observation period (Fig. 4 c). Histological analysis of ear sections at 22 h after allergen exposure also confirmed the enhanced swelling in KO mice (Fig. 4 d). Both visual inspection of the back skin (Fig. 4 e) and spectrophotometric quantification of Evans blue dye extracted from the reaction site of

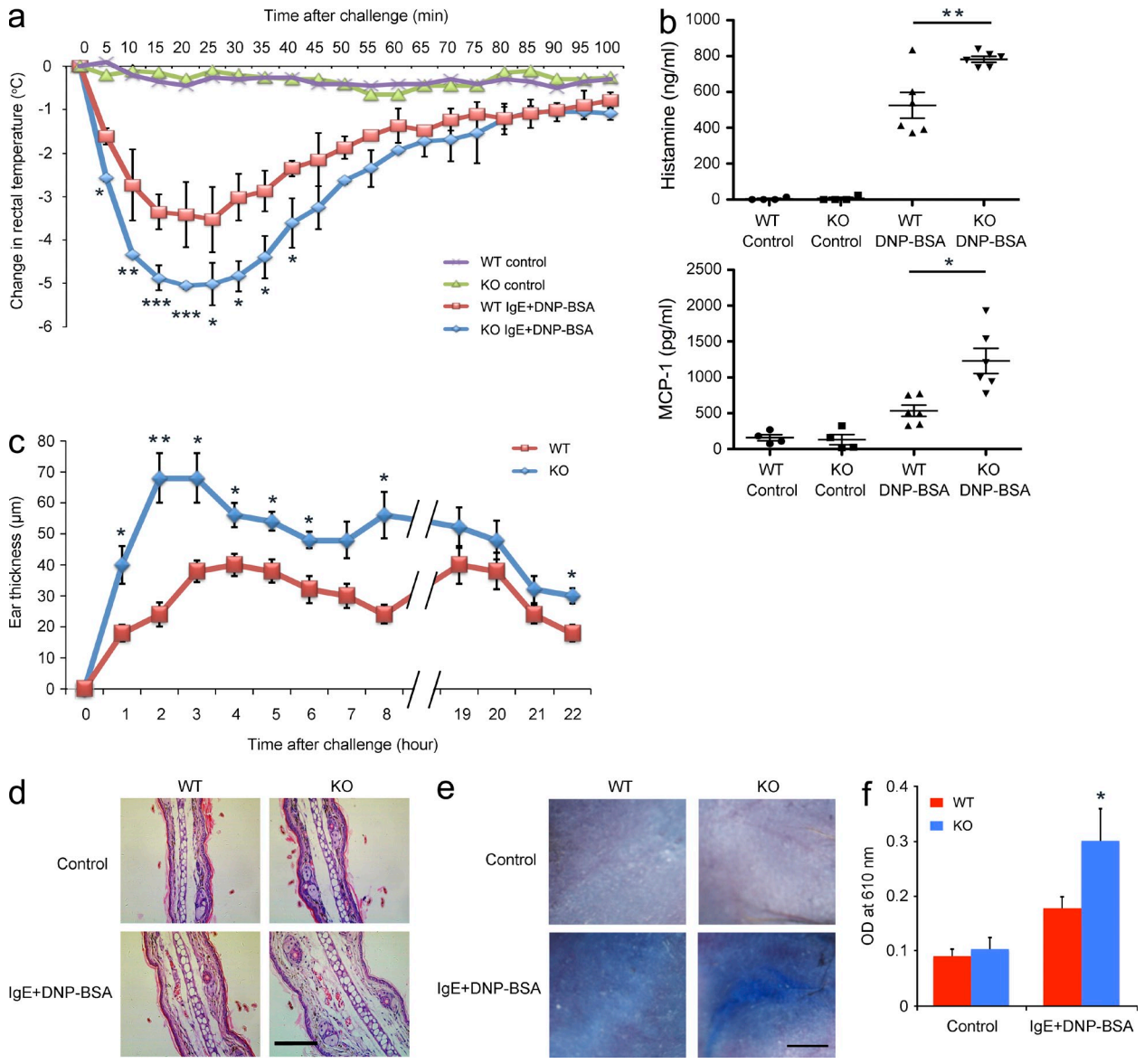

Figure 4. Systemic anaphylaxis and PCA in WT and Tespa1-deficient mice. (a) Mice (n = 6 per genotype) were injected intravenously with anti-DNP IgE, and then challenged 24 h later with PBS or DNP-BSA. Rectal temperatures were assessed every 5 min. (b) Serum levels of histamine and MCP-1 were measured at 100 min after PBS or DNP-BSA challenge. (c) Mice were sensitized by intradermal injection of anti-DNP IgE (left ear) or PBS (right ear), and then challenged 24 h later with DNP-BSA in PBS/Evans blue. Ear swelling was calculated as the difference between the thickness of the right and left ears (n = 6 per genotype). (d) Histological sections of the right (control) and left ears (DNP-BSA) of mice treated as in c, stained with H&E. Bar, 0.2 mm. (e) Mice were sensitized intradermally with anti-DNP IgE or PBS, and then challenged 24 h later with DNP-BSA in PBS/Evans blue and skin was examined visually (n = 6 per genotype). Bar, 2.5 mm. (f) Evans blue dye was extracted in formaldehyde from the reaction sites in e, and quantified as absorbance at 610 nm. *, $P < 0.05$; **, $P < 0.01$; ***, $P < 0.001$ (Student's t test). Data are representative of three (a–d) or two (e and f) experiments (mean and SD in a–c and f).

back skin (Fig. 4 f) demonstrated an enhanced PCA response in KO mice compared with WT controls.

To confirm that our in vivo findings resulted from Tespa1 deficiency in mast cells, PSA experiments were introduced in mast cell–deficient *Kit*$^{w\text{-}sh/w\text{-}sh}$ C57BL/6 mice reconstituted with either WT or KO BMMCs for 16 wk. The mice reconstituted with KO BMMCs showed a significantly enhanced PSA compared with the mice reconstituted with WT BMMCs, despite similar mast cell reconstitution by both WT and KO cells as judged by histological enumeration after toluidine blue staining in the mesenteric window and glandular stomach (Fig. 5, a–c). Collectively, these data suggested that Tespa1 negatively regulates IgE-mediated mast cell activation in vivo and therefore suppresses the anaphylactic responses.

To further clarify the role of Tespa1 in the pathogenesis of other allergic diseases, we used a mast cell–dependent airway inflammation model. According to the established protocol (Williams and Galli, 2000; Izawa et al., 2012), mice received

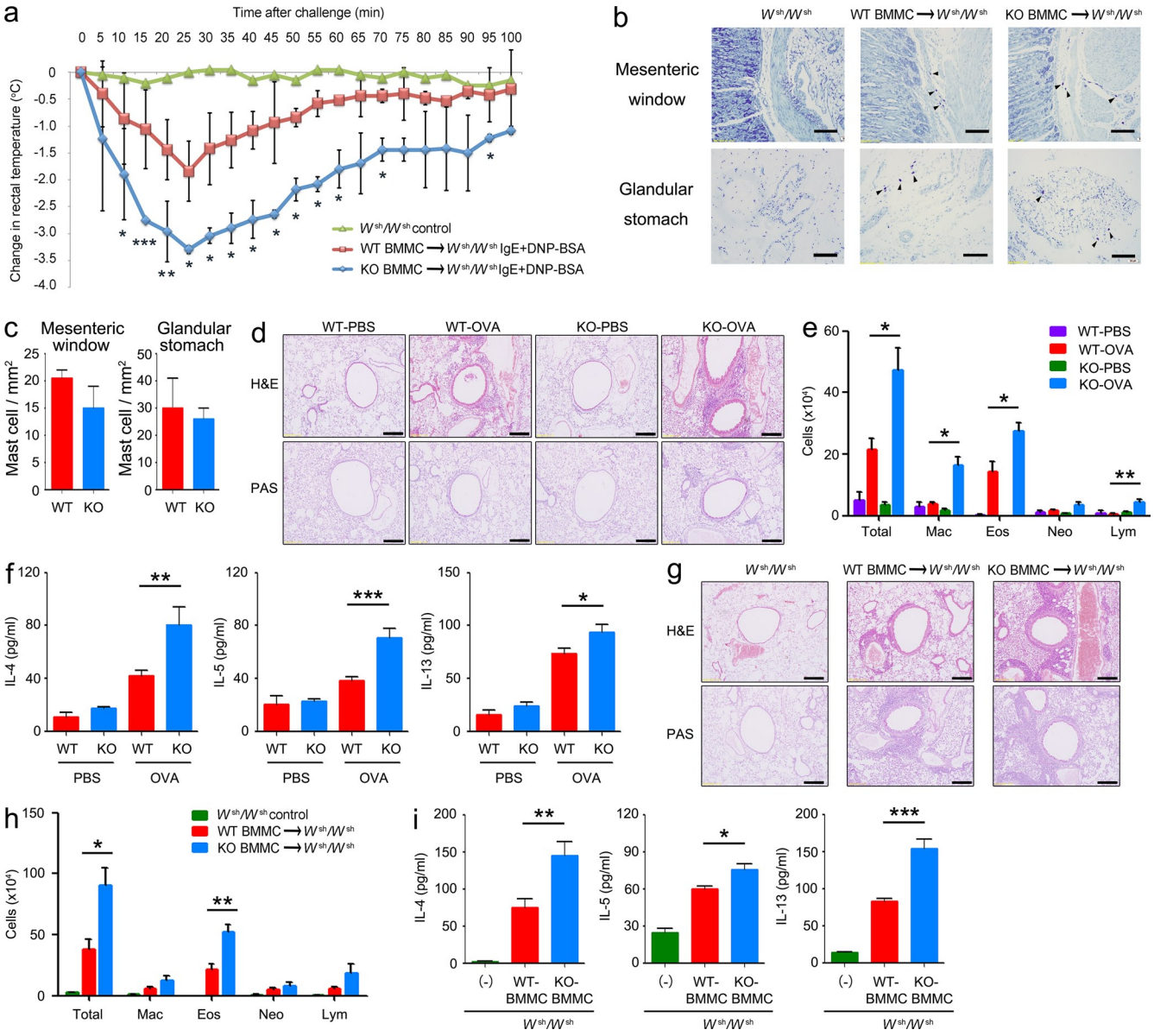

Figure 5. Systemic anaphylaxis and the OVA-induced allergic response in mast cell–reconstituted W^{sh}/W^{sh} mice. (a) Mast cell–deficient mice were given no BMMCs (W^{sh}/W^{sh} control; $n = 2$) or were reconstituted with BMMCs from Tespa1 WT mice (WT BMMC→W^{sh}/W^{sh}; $n = 6$) or KO mice (KO BMMC→W^{sh}/W^{sh}; $n = 6$). 16 wk later, mice were sensitized with 10 µg anti-DNP IgE, followed by challenge with 100 µg DNP-BSA. Rectal temperature was monitored every 5 min. (b) Tissue mast cells in the mesenteric window and glandular stomach from the indicated chimeric mice were assessed toluidine blue staining. Arrowheads indicate individual mast cells. Bars, 100 µm. (c) Absolute numbers of mast cells per mm² (mean and SD). WT and KO mice ($n = 6$ mice per group; d–f) or chimeric mice ($n = 5$ per group; g–i) were sensitized with OVA. Mice were challenged with OVA or PBS in the airway inflammation model and analyzed 24 h after the final challenge. (d and g) Sections of lung tissues were stained with hematoxylin and eosin (H&E). Bars, 100 µm. (e and h) Numbers of total cells (total), eosinophils (Eos), neutrophils (Neu), lymphocytes (lym), and macrophages (Mac) in BALF. (f and i) Amounts of IL-4, IL-5, and IL-13 in BALF as measured by ELISA. Data are representative of two independent experiments. *, $P < 0.05$; **, $P < 0.01$; ***, $P < 0.001$ (Student's t test).

an intranasal challenge with OVA after sensitization to OVA without adjuvant. Hematoxylin and eosin (H&E) and periodic acid-Schiff (PAS) staining revealed increased peribronchiolar inflammatory cell infiltration and enhanced hyperplasia of mucus-secreting goblet cells (PAS^+) in medium and large bronchioles from KO mice (Fig. 5 d).Tespa1 deficiency also increased the inflammatory cells accumulated in the bronchoalveolar fluid (BALF) from challenged mice (Fig. 5 e). In addition, KO mice exhibited more IL-4, IL-5, and IL-13 in BALF than WT mice (Fig. 5 f). $Kit^{w\text{-}sh/w\text{-}sh}$ C57BL/6 mice intravenously transplanted with WT or KO BMMCs were also used 16 wk after transplantation. KO mast cell–reconstituted $Kit^{w\text{-}sh/w\text{-}sh}$ mice exhibited enhanced airway inflammation as evidenced by H&E and PAS staining (Fig. 5 g). KO mast cell–reconstituted

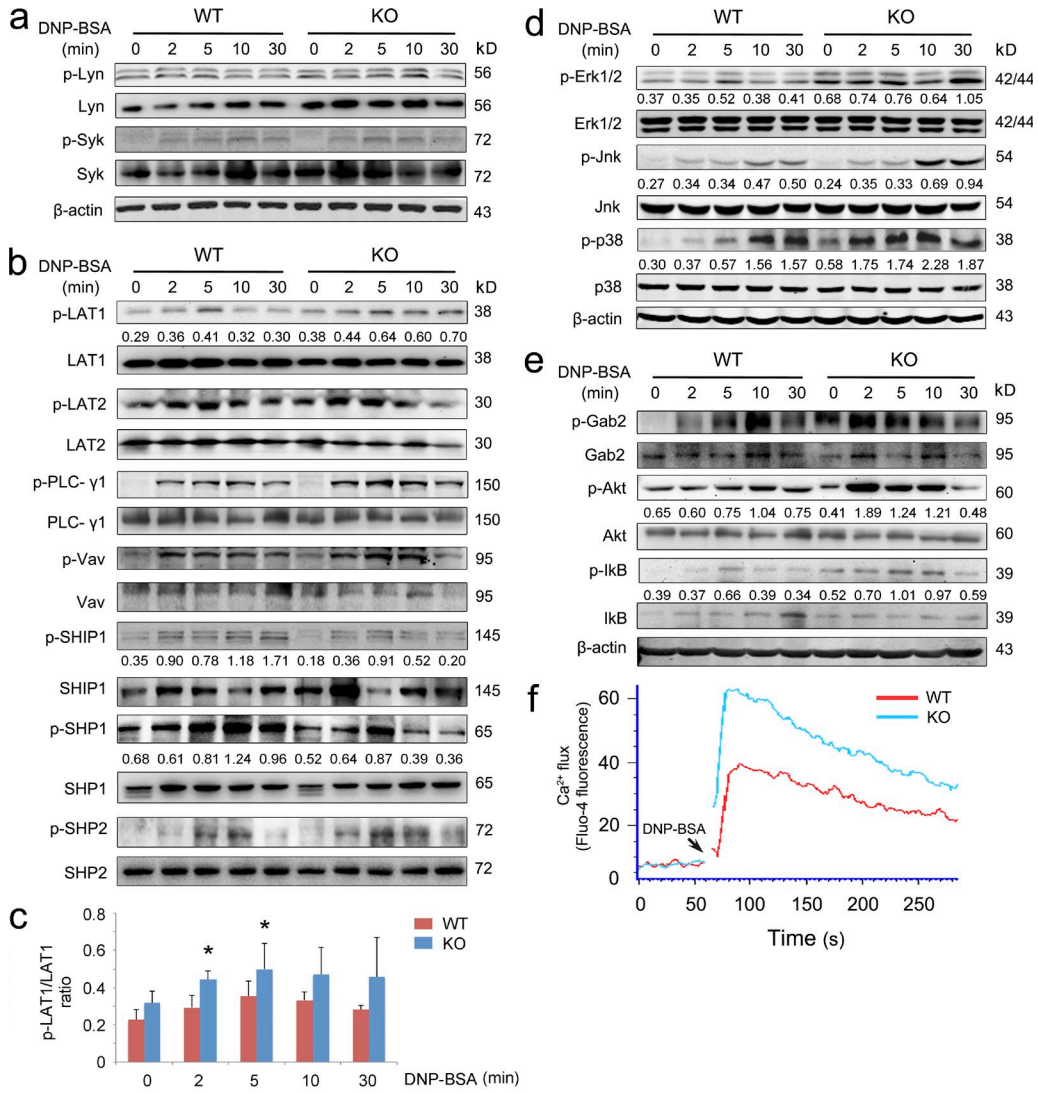

Figure 6. FcεRI-mediated cell signaling in Tespa1 WT and KO BMMCs. (a–c) Levels of phosphorylated Lyn and Syk (a); total and phosphorylated LAT1, LAT2, PLC-γ1, Vav, SHIP1, SHP1, and SHP2 (b); and phosphorylated LAT1 (c) were measured by immunoblot. Phospho-LAT1 was normalized to total LAT1 by densitometry statistical analysis. Error bars represent SD. (d–f) BMMCs were sensitized with anti-DNP IgE and then stimulated with DNP-BSA for 2, 5, 10, or 30 min or left unstimulated. (d and e) Total and phosphorylated Erk, Jnk, and p38 (d); and total and phosphorylated Gab2, Akt, and IκB (e) in cell extracts were assessed by immunoblot. (f) Calcium flux was measured at the indicated times after stimulation. Data are representative of three experiments. *, $P < 0.05$.

Kit$^{w\text{-}sh/w\text{-}sh}$ mice also showed greater numbers of inflammatory cells in BALF, caused primarily by increased eosinophils (Fig. 5 h), and increased levels of cytokines in BALF compared with WT mast cell–reconstituted *Kit*$^{w\text{-}sh/w\text{-}sh}$ mice (Fig. 5 i).

Altered FcεRI signaling events in KO BMMCs

The data above indicated that Tespa1 negatively regulates FcεRI-mediated mast cell activation both in vitro and in vivo. We next examined the activation of intracellular signaling pathways by FcεRI in WT and KO BMMCs. Mast cells were sensitized with anti-DNP IgE, followed by DNP-BSA cross-linking for different time periods before Western analysis. The overall tyrosine phosphorylation and activation status of the FcεRI-proximal tyrosine kinases Lyn and Syk were not significantly changed in mast cells derived from WT and KO mice (not depicted and Fig. 6 a). Next, we detected the phosphorylation of both LAT1 and LAT2 after FcεRI engagement. LAT1 phosphorylation was slightly higher in KO BMMCs after stimulation (Fig. 6 b). Statistical densitometric analysis of three experiments revealed an increase in the phosphorylation of LAT1 in KO BMMCs at 2 and 5 min after stimulation (Fig. 6 c). However, the phosphorylation of LAT2 remained unaltered in the absence of Tespa1 (Fig. 6 b). In addition, a mild change of PLC-γ1 and Vav phosphorylation in KO BMMCs was also found (Fig. 6 b). Interestingly, Tespa1 deficiency resulted in subtly decreased phosphorylation of the phosphatases SHIP1 and SHP1, which can negatively regulate mast cell activation (Gilfillan and Tkaczyk, 2006; Fig. 6 b). Moreover,

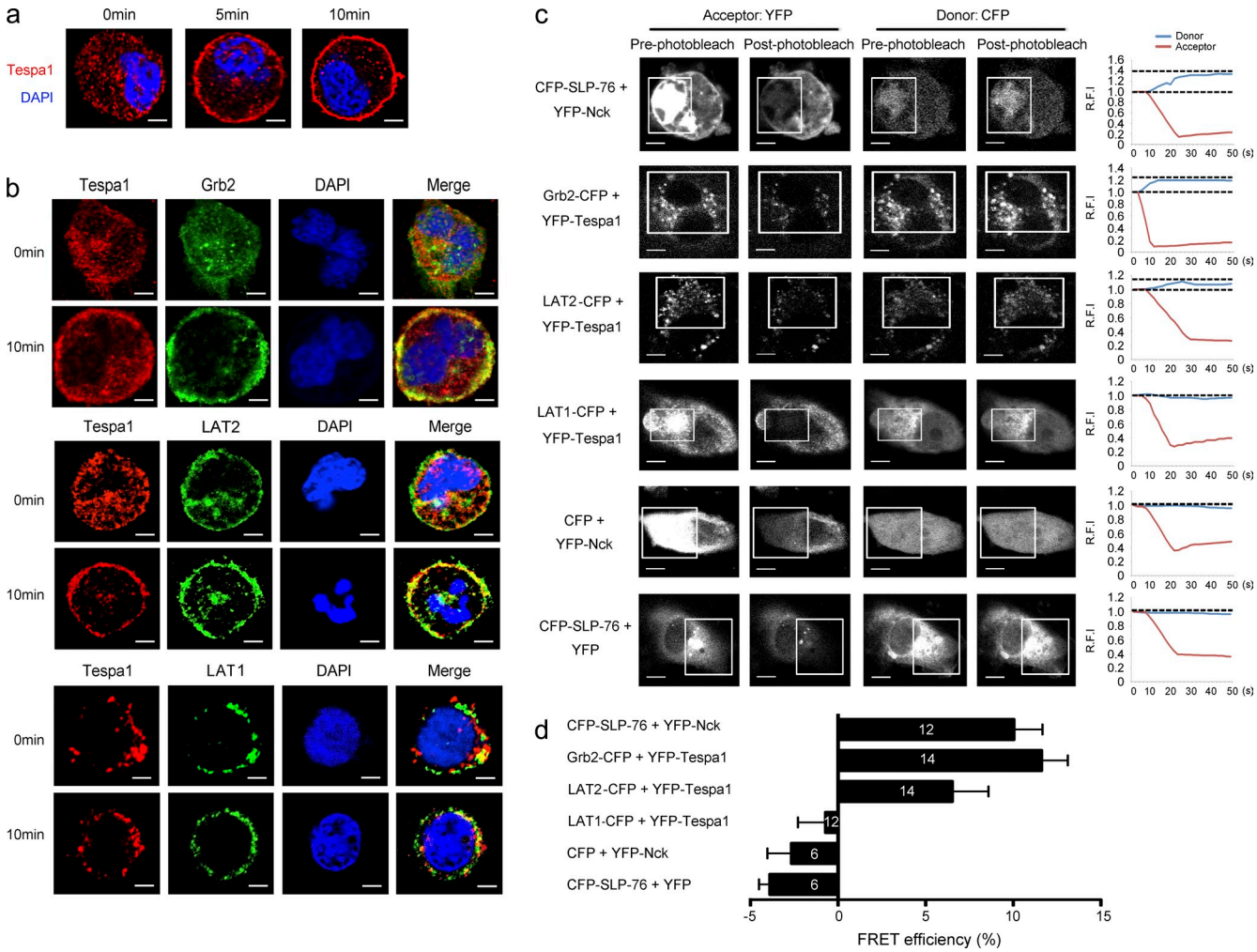

Figure 7. Involvement of Tespa1 in FcεRI-mediated LAT2 signalosome assembly and preferential binding of Tespa1 with LAT2 versus LAT1. (a) BMMCs were sensitized with anti-DNP IgE and labeled with anti-Tespa1 (red) and DAPI (blue) before (0 min) and after (5 and 10 min) of stimulation. Bars, 2 µm. (b) BMMCs stimulated as in a were labeled with anti-Tespa1 (red), anti-Grb2 (green, top group), LAT2 (green, middle group), or anti-LAT1 (green, lower group) and DAPI (blue) before (0 min) and after (10 min) stimulation. Bars, 2 µm. (c) Live COS-7 cells transfected with the indicated pairs of CFP- and YFP-bearing constructs and analyzed by acceptor photobleaching FRET microscopy. White boxes indicate the bleached region. Group (right), donor, and acceptor relative fluorescence intensities were monitored in the bleached regions and plotted over time. Bars, 15 µm. (d) Average FRET efficiency obtained from acceptor photobleaching. White numbers in the bar graph indicate the numbers of cells used for FRET measurement. Detectable FRET between CFP-SLP-76 and YFP-Nck was taken as positive control; little or no detectable FRET between YFP-Nck and free CFP or between CFP-SLP-76 and free YFP were taken as negative controls. Data are representative of at least three experiments.

a slightly increased SHP2 phosphorylation was also found in the absence of Tespa1, which is considered to be a positive regulator of FcεRI signaling (Brockmeyer et al., 2011; Paster et al., 2013; Fig. 6 b). Compared with the aforementioned subtle changes of phosphorylation, Tespa1 deficiency resulted in a more striking enhancement in the activation of distal signaling, including the activation of the mitogen-activated protein kinases Erk, Jnk, and p38 (Fig. 6 d), which are widely reported to be critical for the FcεRI-dependent cytokine and chemokine production by mast cells (Teramoto et al., 1997; Saitoh et al., 2003; Gilfillan and Tkaczyk, 2006). To our great surprise, the phosphorylation of FcεRI-induced complementary axis downstream molecules—Akt and the inhibitor IκB—was also markedly increased in Tespa1-deficient BMMCs. In addition, the phosphorylation of Gab2 was more rapidly increased in KO BMMCs than in WT BMMCs (Fig. 6 e). These data suggested perturbation of both the FcεRI-induced principal axis (Grb2/PLC-γ1/SLP-76/MAPK) and the complementary axis (Gab-2/PI3K/Akt) in the absence of Tespa1.

A transient increase of intracellular calcium is essential for the degranulation in mast cells after allergen exposure (Gilfillan and Tkaczyk, 2006; Baba et al., 2008). Both the principle and complementary axis could influence the calcium influx during mast cell activation. As expected, we found that BMMCs from KO mice had much higher levels of FcεRI-elicited calcium flux than did WT BMMCs (Fig. 6 f), consistent with the enhanced

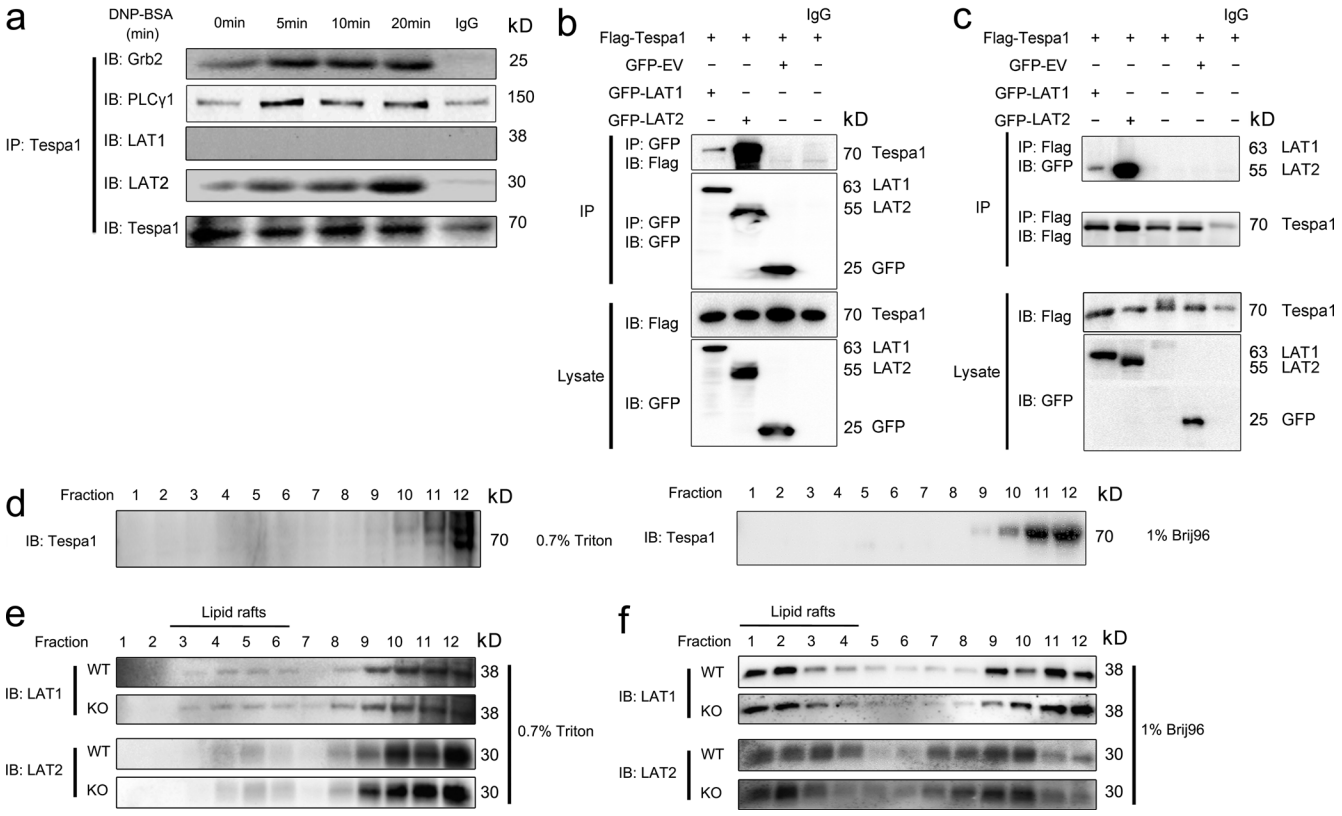

Figure 8. Preferential binding of Tespa1 with LAT2 versus LAT1. (a) Tespa1 WT BMMCs were sensitized with anti-DNP IgE and then left unstimulated (0 min) or stimulated for 5, 10, or 20 min with DNP-BSA. Cells were lysed, and immunoprecipitated (IP) with anti-Tespa1, and probed with anti-Grb2, anti–PLC-γ1, anti-Lat, anti-LAT2, or anti-Tespa1 and analyzed by immunoblotting. (b) HEK-293 cells were transfected with Flag-Tespa1 and GFP-EV (empty vector), GFP-LAT1, or GFP-LAT2 plasmid as indicated, then lysed and immunoprecipitated (IP) with anti-Flag or mouse IgG (control) and probed with anti-GFP or anti-Flag. Below, immunoblot analysis of lysates (without immunoprecipitation) with anti-Flag or anti-GFP. Data are representative of at least three experiments. (c) BMMCs were stimulated as in a and immunoprecipitated (IP) with anti-FLAG or mouse IgG (control) and probed with anti-GFP or anti-Flag. Below, immunoblot analysis of lysates (without immunoprecipitation) with anti-Flag or anti-GFP. (d) Localization of Tespa1 in WT mast cells. BMMCs from WT mice were lysed in 0.7% Triton or 1% Brij96 before ultracentrifugation on a sucrose gradient. 12 fractions were collected starting from the top of the sucrose gradient. Each fraction was resolved on SDS-PAGE and blotted with anti-Tespa1. (e and f) Localization of LAT1 and LAT2 in WT and Tespa1-deficient mast cells. BMMCs were lysed in 0.7% Triton (e) or 1% Brij96 (f) before ultracentrifugation on a sucrose gradient. 12 fractions were collected starting from the top of the sucrose gradient. Each fraction was resolved on SDS-PAGE and blotted with anti-LAT1 and anti-LAT2 antibodies. Data are representative of at least three experiments.

degranulation in KO BMMCs. In sum, these data suggested that the negative regulation of mast cell activation by Tespa1 involves changes in FcεRI signaling.

Preferential association of Tespa1 with LAT2, rather than with LAT1, in mast cell activation

Although the interplay between the LAT1 and LAT2 signalosomes is still not clear, with the previous paradoxical data (Alvarez-Errico et al., 2009; Fu et al., 2009), many reports converge to a model suggesting that both LAT1 and LAT2 could facilitate the principle axis (Grb2/PLC-γ1/SLP-76/Vav), but the complementary axis (Gab-2/PI3K/Akt) in mast cell activation mainly depends on LAT2 (Rivera, 2005; Gilfillan and Tkaczyk, 2006; Alvarez-Errico et al., 2009). Based on perturbation of both the principal and complementary axes in Tespa1-deficient BMMCs, we speculate that Tespa1 might preferentiality orchestrate the assembly of both the LAT1 and LAT2 signalosomes, facilitating either the principal or the complementary signaling pathway. To test this speculation, we first observed the subcellular localization of Tespa1 in mast cells. Confocal microscopy showed a dispersed pattern of Tespa1 in the cytosol of ready-state sensitized BMMCs. After stimulation with DNP-BSA for 5 and 10 min, Tespa1 clearly translocated to the plasma membrane (Fig. 7 a) and showed substantial colocalization with Grb2 and LAT2 by 10 min, which suggested that Tespa1 might be involved in the LAT2 signalosome upon FcεRI engagement in mast cells. To a less extent, we also observed colocalization of Tespa1 and LAT1 by 10 min after mast cell activation (Fig. 7 b). To confirm this binding preference, we then used a fluorescence resonance energy transfer (FRET) assay to assess the relative proximity of Tespa1 and LAT1 or LAT2 in live cells. In COS-7 cells, coexpression of YFP-Tespa1 and Grb2-CFP produced FRET, which demonstrated an association between Tespa1 and Grb2 (Fig. 7, c and d). More

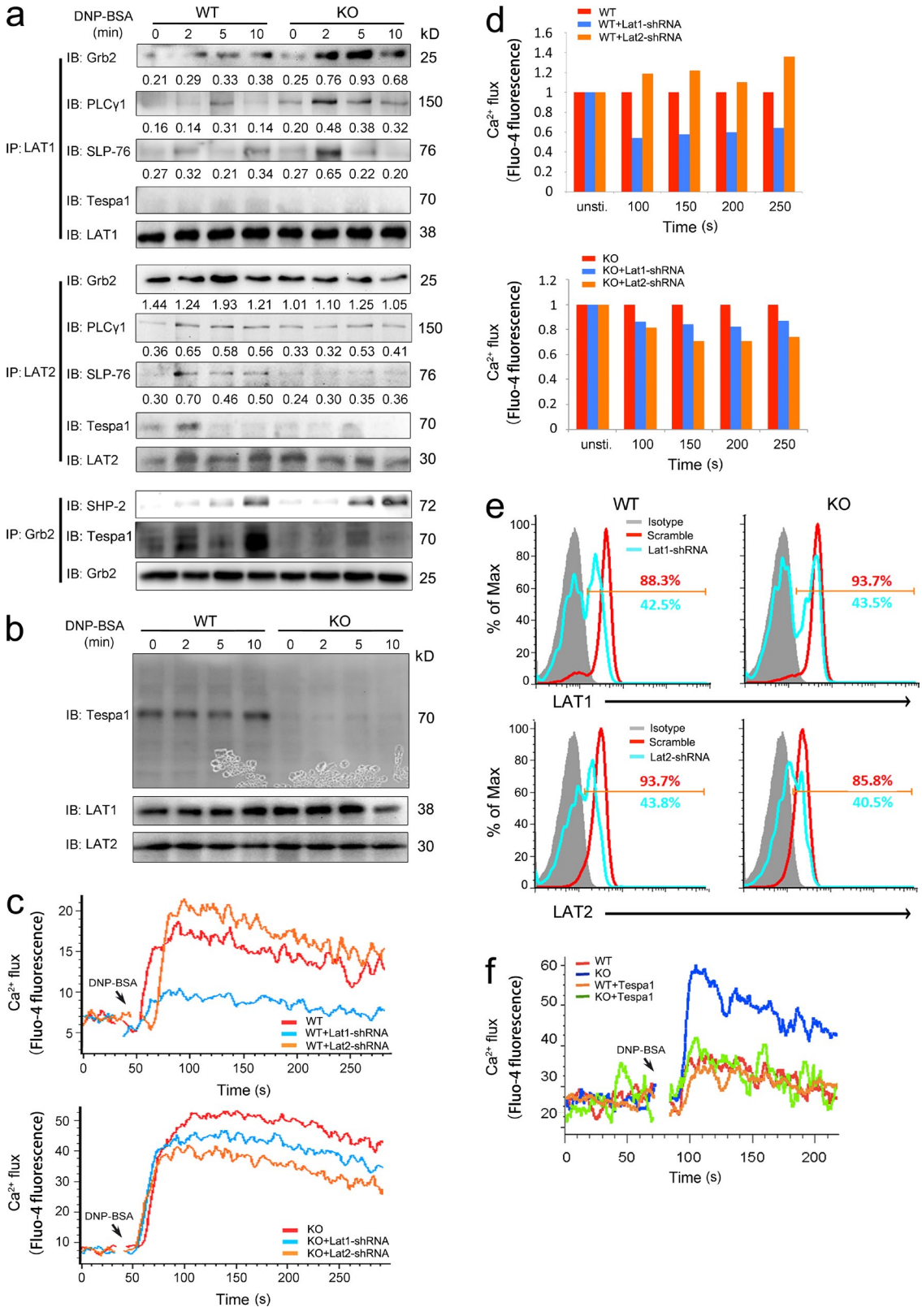

Figure 9. FcεRI-mediated LAT1 and LAT2 signalosome assembly in Tespa1-deficient BMMCs. (a) Tespa1 WT and KO BMMCs were sensitized with anti-DNP IgE and left unstimulated (0 min) or stimulated for 2, 5, or 10 min, then lysed, immunoprecipitated (IP) with anti-LAT1 (top), anti-LAT2 (middle), or anti-Grb2 (bottom), and probed with anti-Grb2, anti-PLC-γ1, anti–SLP-76, anti-Tespa1, anti-LAT1, anti-LAT2, or anti-SHP2. (b) BMMCs were sensitized as in a, left unstimulated (0 min) or stimulated for 2, 5, or 10 min, and then lysed and immunoblotted with anti-Tespa1, anti-LAT1, and anti-LAT2. (c) Tespa1 WT

importantly, coexpression of YFP-Tespa1 and LAT2-CFP produced significantly greater FRET than did coexpression of YFP-Tespa1 and LAT1-CFP, indicating that Tespa1 was in close proximity to LAT2 but not LAT1 in living cells (Fig. 7, c and d). Detectable FRET between CFP-SLP-76 and YFP-Nck was taken as a positive control, and little or no detectable FRET between YFP-Nck and free CFP or between CFP-SLP-76 and free YFP was taken as a negative control (Fig. 7, c and d). To further determine which signalosome Tespa1 was involved with, we next performed coimmunoprecipitation analysis. The results showed that Tespa1 associated with Grb2 and PLC-γ1 after DNP-BSA stimulation in a time-dependent manner in BMMCs. Strikingly, prolonged FcεRI engagement also induced an enhanced association of Tespa1 with LAT2 but not with LAT1 in BMMCs, which suggested the preferential involvement of Tespa1 with the LAT2 signalosome during mast cell activation (Fig. 8 a). When we cotransfected Flag-Tespa1 with both GFP-LAT1 and GFP-LAT2 in HEK293 cells, we also found that the association of Tespa1 with LAT2 is much more than that with LAT1, regardless of the precipitation antibody (anti-Flag or anti-GFP; Fig. 8, b and c). These data provided direct evidence that Tespa1 preferentially associates with LAT2 rather than LAT1 in both cell lysates and living cells.

Tespa1-deficient BMMCs show skewed LAT1 signalosome assembly compared with LAT2 upon FcεRI stimulation

The data above suggested the involvement of Tespa1 in the LAT2 signalosome. We next checked whether it could orchestrate the synergy and balance between LAT2 and LAT1 signalosome-related individual downstream signaling events. We first showed that Tespa1 was mainly expressed in the non-lipid rafts of BMMCs (Fig. 8 d). Then we observed the localization of LAT1 and LAT2 to lipid rafts in WT and KO BMMCs but found no substantial differences either in Triton- or Brji 96–solubilized cells (Fig. 8, e and f). However, in subsequent coimmunoprecipitation assays to detect the assembly of principal axis–related signaling molecules, we found that Tespa1 deficiency led to more Grb2, PLC-γ1, and SLP-76 associated with LAT1 but less association with LAT2 upon FcεRI stimulation (Fig. 9 a). Again, we detected an association between LAT2 and Tespa1 at an early time point after BMMC stimulation but not an obvious association between LAT1 and Tespa1 (Fig. 9 a). We also found a very mildly increased association between SHP2 and Grb2, which suggested a limited contribution of SHP2 to the phenotype of Tespa1-deficient BMMCs (Fig. 9 a). It has been reported that Tespa1 protein in T cells is retarded toward a high molecular weight area on the immunoblot upon treatment with ionomycin, which suggests a modification of Tespa1 protein during signaling transduction (Fujimoto et al., 2013). To confirm whether a similar retardation of Tespa1 protein occurred in our system, we used the whole blot for detection with our Tespa1 antibody. The result showed no evident retardation of Tespa1 protein on the immunoblot upon FcεRI stimulation (Fig. 9 b). To further confirm the contribution of this skewed signalosome assembly in KO cells to LAT1- and LAT2-mediated signaling, we next used lentivirus-mediated RNA interference to knock down LAT1 and LAT2 individually in both WT and KO BMMCs. Consistent with previous reports, LAT1 knockdown in WT BMMCs impaired the calcium release but LAT2 knockdown enhanced it. On the contrary, in KO BMMCs, both LAT1 and LAT2 knockdown decreased the calcium release, which indicated that the balance between LAT1 and LAT2 signalosomes is disrupted in the absence of Tespa1 (Fig. 9, c and d). The reduced percentage decrease of calcium flux caused by LAT1 knockdown in the absence of Tespa1 could be the result of an overcompensated LAT1 signalosome in KO BMMCs. We also noted that LAT2 knockdown caused a more overtly decreased calcium flux compared with LAT1 knockdown in *Tesap1*$^{-/-}$ BMMCs, which suggested that the LAT2-related complementary axis might also be strengthened in the absence of Tespa1. The similar knockdown efficiencies of *lat1* and *lat2* in WT and KO BMMCs were determined by flow cytometry (Fig. 9 e). Last, to further confirm the contribution of Tespa1 protein to the unexpected phenotype of Tespa1-deficient BMMCs, we performed a rescue experiment. The overexpression of Tespa1 in *Tesap1*$^{-/-}$ BMMCs by nucleofection reverted the increased FcεRI-mediated calcium flux to the level of WT BMMCs (Fig. 9 f). In sum, these data indicated that Tespa1 deficiency induces skewed LAT1 signalosome assembly compared with that of the LAT2 signalosome upon FcεRI stimulation, thus enhancing the final FcεRI signaling outcome.

DISCUSSION

Here, we have described an unexpected negative regulatory function of Tespa1 in FcεRI-mediated mast cell activation and allergic responses. The absence of Tespa1 did not affect the development of mast cells but caused them to be hyperresponsive to stimulation via FcεRI both in vitro and in vivo.

FcεRI-mediated mast cell activation is negatively regulated by several inhibitory mechanisms. The orchestration of the intracellular molecules involved in FcεRI signaling executes delicate negative regulation during mast cell activation, and this is critical for preventing excessive inflammation and allergic response. For example, Lyn kinase is thought to be

(top) and KO (bottom) BMMCs transfected with control vector, Lat1-shRNA, or Lat2-shRNA plasmid were stimulated with DNP-BSA, and then Ca^{2+} flux was monitored at indicated time points after stimulation. (d) Tespa1 WT (top) and KO (bottom) BMMCs transfected with control vector, Lat1-shRNA, or Lat2-shRNA plasmid and were sensitized with anti-DNP IgE then left unstimulated or stimulated for 100, 150, 200, or 250 s with DNP-BSA (mean Fluo-4 fluorescence of BMMCs transfected with control vector set at 1). Ca^{2+} flux was monitored at indicated time points after stimulation. (e) *Lat1* and *Lat2* expression were silenced in Tespa1 WT and KO BMMCs by lentivirus-mediated RNA interference. (f) Tespa1 WT and KO BMMCs were nucleofected with Tespa1 plasmid for overexpression and were sensitized with anti-DNP IgE then stimulation with DNP-BSA. Data are representative of three experiments.

required for mast cell activation by its ability to phosphorylate several key mediators, but it also negatively regulates FcεRI signaling by competing with another kinase, Fyn, and activating SHIP1 phosphatase (Gilfillan and Tkaczyk, 2006). The balance between the LAT1 and LAT2 signalosomes also contributes greatly to the final outcome of FcεRI signaling. Both LAT1 and LAT2 could be phosphorylated by upstream tyrosine kinases and provide potential docking sites for several common and unshared molecules such as Grb2 and Gab2. Our data showed that Tespa1 had priority in associating with LAT2 and facilitated the binding of these signaling molecules with LAT2. In the absence of Tespa1, the binding of the signaling molecules Grb2, PLC-γ1, and SLP-76 shifted from LAT2 to LAT1, which led to overcompensation of the LAT1 signalosome. At the same time, the vacated potential docking sites on LAT2 might provide an increased binding probability for Gab2 and PI3K, which facilitated the complementary signaling pathway, thus providing another possibility of increased complementary signaling through the enhanced phosphorylation of Gab2. In addition, the contribution of certain phosphatases such as SHIP1 and SHP1 could also be involved in the hypersensitive phenotype in Tespa1-deficient BMMCs.

However, we cannot exclude the possibility that Tespa1 could also deliver a positive signaling based on its function in T cell development and its association with Grb2 signalosome, although this impact might be masked by the overwhelming opposite phenotype in Tespa1-deficient BMMCs. Moreover, except for its enriched expression in T cells and mast cells, Tespa1 was also highly expressed in B cells, which might endow the different, even opposite functions of Tespa1 in distinct cell types and physiological contexts.

We have shown that Tespa1 preferentially binds to LAT2 but not LAT1 in mast cells, and loss of Tespa1 impairs formation of the LAT2 signalosome. In naive T cells, without LAT2 expression, Tespa1 might be involved in the LAT1 signalosome by its interaction with other adaptor proteins such as Grb2 or PLC-γ1. But in mast cells, LAT2 has binding priority with Tespa1 to control their moderate activation. However, the precise function of Tespa1 in LAT1 or LAT2 signalosome assembly remains an open question. We found that Tespa1 bound directly to PLC-γ1 but not other signalosome components in the yeast two-hybrid assay (unpublished data), which provides a possible explanation. It is already known that LAT2 lacks a direct PLC-γ1–binding site like LAT1 and recruits PLC-γ1 in an indirect manner. This was originally thought to be mediated by phosphorylated Grb2. But the mediation by Grb2 cannot explain the differential allocation of the signaling components to the two different signalosomes because Grb2 binds to both LAT1 and LAT2. Thus, the specific recruitment of PLC-γ1 onto LAT2 by Tespa1 provides an attractive model to settle this long-lasting controversy.

A very recent study demonstrated that FcεRI could discriminate high- from low-affinity stimulation to modulate the events of mast cell activation including receptor cluster size, mobility, distribution, and the cells' effector responses (Suzuki et al., 2014). This raises the possibility that Tespa1 might also be involved in the discrimination between high- and low-affinity stimulation mediated different downstream events of mast cell activation through fine-tuning the balance between LAT1 and LAT2.

Compared with the clear phenotype and signaling changes due to Tespa1 deficiency, the molecular mechanism underlying the preferential binding of Tespa1 is still obscure. Sequence analysis suggested that Tespa1, unlike typical other adaptors, lacks conserved protein–protein interaction domains such as SH2 and SH3. There is a potential SH3-binding PPP site and several potential myristoylation sites at the N terminus which might be related to its membrane targeting and signal transduction. It has been reported that Tespa1 directly interacts with inositol 1,4,5-trisphosphate receptor, facilitating the TCR stimulation-induced calcium flux into both cytoplasm and mitochondria (Matsuzaki et al., 2013). This is incompatible with the phenotype of enhanced FcεRI-mediated calcium flux in the absence of Tespa1. The different cell type or a different stimulus affinity might explain this inconsistency. In addition, previous data showed that the phosphorylation of different individual tyrosine residues might endow distinct recruiting ability of LAT1 and LAT2 to form individual signalosomes and the subsequent signaling outcome (Gilfillan and Tkaczyk, 2006). More work is needed to understand the connection between the individual phosphorylated tyrosine residues of LAT1/LAT2, the individual phosphorylated tyrosine residues of Tespa1, and their binding preference in FcεRI-induced signalosome assembly.

In sum, our findings put Tespa1 in a key position in the regulation of FcεRI signaling and mast cell–mediated allergic responses. In mast cells, Tespa1 works as an adjusting lever to determine the allocation of signaling molecules to either the LAT2 or the LAT1 signalosome. The preferential assembly of the LAT2 signalosome promoted by Tespa1 might serve as a reservoir to regulate the signal strength of LAT1, i.e., absorbing the signal molecules when the LAT1 signal is too strong, and releasing signals when the LAT1 signal is missing or insufficient. The mast cell plays a key and connective function during allergic pathogenesis. Based on the orchestrating function of Tespa1 in mast cell activation, it can be speculated that the absence, reduced expression, or mutations in this adaptor protein might be a contributing factor in an increased sensitivity to allergens. This thus raises the possibility that strategies to fine-tune the Tespa1 levels might have therapeutic benefits in atopic individuals.

MATERIALS AND METHODS

Mice. *Tespa1*$^{-/-}$ mice were generated by homologous recombination-mediated gene targeting at the Shanghai Research Center for Model Organisms as previously described (Wang et al., 2012). Mice on a mixed 129 × C57BL/6 background were backcrossed onto the C57BL/6 background for 6–8 generations. *Kit*$^{w\text{-}sh/w\text{-}sh}$ mice were from The Jackson Laboratory. All mice were housed in the University Laboratory Animal Center. Animal experiment protocols were approved by the Review Committee of Zhejiang University School of Medicine and were in compliance with institutional guidelines.

Antibodies. FITC-conjugated antibody to mouse CD117 (c-kit) and CD107a, and PE-conjugated antibody to mouse FcεRI, were from BioLegend.

Anti–Erk1-Erk2 (9102), antibody to Erk1-Erk2 phosphorylated at Thr202 and Tyr204 (9101), anti–Jnk1-Jnk2 (56G8), antibody to Jnk1-Jnk2 phosphorylated at Thr183 and Tyr185 (9251), anti-p38 (9212), antibody to p38 phosphorylated at Thr180 and Tyr182 (9211), anti-Akt (C67E7), antibody to Akt phosphorylated at Ser473 (D9E), antibody to Zap70 phosphorylated at Tyr319 and Syk phosphorylated at Tyr352 (2701), anti-IκB (44D4), antibody to IκB phosphorylated at Ser32 and Ser36 (5A5), anti-Lyn (2732), anti-SHIP1 (D1163), antibody to SHIP1 phosphorylated at Tyr1020 (3941), anti-SHP1 (C14H6), and antibody to SHP1 phosphorylated at Tyr564 (D11G5) were from Cell Signaling Technology. Anti-Grb2 (Y237), anti–PLC-γ1 (EP1898-7Y), anti-SLP76 (EPR2549), antibody to PLC-γ1 phosphorylated at Tyr 783 (EP1898Y), antibody to Lyn phosphorylated at Tyr507 (EP504Y), antibody to LAT1 phosphorylated at Tyr191 (E225) anti-SHP2, and antibody to SHP2 phosphorylated at Tyr542 (EP508(2)Y) were from Epitomics. Anti-LAT1 (11B.12), LAT2 (NAP-07), and anti-Syk (SYK-01) were from BioLegend. Monoclonal antibody to mouse and human Tespa1 were custom made by Abmart.

Cell cultures. For BMMCs, mouse BM cells were isolated from femurs and cultured in RPMI medium plus 10% (vol/vol) FBS (Gibco) with 10 ng/ml IL-3 (PeproTech) and 10 ng/ml stem cell factor (PeproTech). Half of the medium was replaced with fresh medium with cytokines every 4–5 d during culture. After 4–6 wk in culture, BMMCs were stained to confirm the surface expression of FcεRI and c-Kit. Cells with purity >95% were used for subsequent experiments. For BM-derived DCs, mouse BM cells were cultured in RPMI medium plus 10% (vol/vol) FBS (Gibco) with 20 ng/ml GM-CSF (PeproTech) and 2 ng/ml IL-4 (PeproTech). Supplemented medium was replaced every 3 d. On day 6, nonadherent and loosely adherent DCs were purified using MACS columns (Miltenyi Biotec). For BM-derived macrophages, mouse BM cells were cultured in RPMI medium plus 10% (vol/vol) FBS (Gibco) with 20 ng/ml M-CSF (PeproTech). On day 4, nonadherent cells were collected and cultured for a further 3 d in the presence of 20 ng/ml of fresh M-CSF (PeproTech). On day 7, adherent cells were collected.

Alcian blue/safranin staining. Cells were cytocentrifuged, air-dried, incubated for 20 min with 0.5% Alcian blue in 0.3% acetic acid, rinsed in water, and incubated for 20 min with 0.1% safranin in 1% acetic acid. Cells were examined under a microscope (IX71; Olympus).

RT-PCR analysis. RT-PCR reactions for evaluation of the expression of IL-3, IL-4, IL-5, IL-9, IL-13, IL-33, IL-1β, IL-6, TNF, GM-CSF, MCP-1, MIP-1α, RANTES, IL-10, IL-2, TGF-β, IFN-γ, IL-2, MCP-5, MCP-6, and β-actin were performed using gene-specific primers. Results were normalized to β-actin expression.

ELISA and Multiplex suspension array. BMMCs were incubated overnight at 37°C with 1 μg/ml IgE anti-DNP in 1 ml culture medium and then stimulated for 24 h at 37°C with 10 ng/ml DNP-BSA. The amount of cytokine in the supernatant was determined using a Multiplex suspension array system (Bio-Rad Laboratories) or standard ELISA according to the manufacturer's instructions.

Degranulation assay. BMMCs were incubated overnight at 37°C with 1 μg/ml IgE anti-DNP in 1 ml culture medium and then stimulated for 1 h at 37°C with 10 ng/ml DNP-BSA antigen in 200 μl Hepes-Tyrode's buffer, pH 7.4. Culture supernatants from both stimulated and unstimulated cells were collected and assayed for β-hexosaminidase as previously described (Orr and McVicar, 2011). For analysis of the total β-hexosaminidase in cell content, cells were lysed with 0.5% (vol/vol) Triton X-100 in Hepes-Tyrode's buffer. The percentage degranulation was calculated as follows: absorbance of culture supernatant at 405 nm × 100/absorbance of total cell lysate supernatant at 405 nm.

LTC4, D4, E4, and histamine release assays. 1×10^6 BMMCs were sensitized with IgE anti-DNP and challenged with 5–100 ng/ml DNP-BSA. Supernatants were collected 1 h after challenge, and LTC4, D4, and E4 were titrated by competitive ELISA (Neogen). Histamine was measured in cells and supernatants using fluorometric assay (Vennekens et al., 2007). The percentage of histamine release was quantified by the following equation: histamine in supernatant/(histamine in supernatant + histamine in pellet) × 100.

Migration assays. Mast cell migration assays were performed using matrix-coated polycarbonate filters (8-μm pore size, 24 wells; Transwell; BD). The membrane undersurface was coated with 100 μg/ml fibrinogen in PBS for 1 h at 37°C and blocked with migration buffer (0.5% BSA in α-MEM) for 30 min at 37°C. IgE 2.5×10^5 anti–DNP-sensitized BMMCs were seeded in the upper wells in 0.2 ml medium and the lower wells were supplied with 0.5 ml medium titrated with different concentrations of DNP-BSA. 6 h later, cells that had migrated into the lower wells were stained with DAPI and counted under a microscope.

Measurement of cell-electrode impedance. The detailed procedures for the xCELLigence system (Roche), also known as the Real-Time Cell Electronic Sensing System (RT–CES; ACEA Biosciences), have been described previously (McPherson et al., 2009). Briefly, the wells were coated with 100 μg/ml fibrinogen in PBS for 2 h at 37°C and blocked with 0.5% BSA for 30 min at 37°C, and then washed three times with PBS. For time-dependent cell response profile measurements, 50 μl of medium was added to 16-well E-plates to obtain background readings, followed by the addition of 100 μl mast cell suspension (6×10^4 cells/well). The E-plates containing the indicated cells were incubated at room temperature for 30 min before being placed onto the reader in the incubator. 1 μg/ml anti-DNP IgE was added to the medium for sensitization. 5 h later, cells were challenged with 100 ng/ml DNP-BSA for 16 h. Impedance as reflected by the CI was recorded continuously.

PSA. WT, Tespa1-deficient, mast cell–deficient ($Kit^{w\text{-}sh/w\text{-}sh}$) and $Kit^{w\text{-}sh/w\text{-}sh}$ mice that had been reconstituted with WT or Tespa1-deficient BMMCs were sensitized by intravenous injection of 10 μg mouse IgE anti-DNP (SPE-7; Sigma-Aldrich) for 24 h and challenged intravenously with 100 μg DNP-BSA. After antigen challenge, rectal temperature was measured and recorded every 5 min for 100 min with a digital thermometer (Omron). For BMMC engraftment experiments, BMMCs from WT and $Tespa1^{-/-}$ mice were cultured, and 6 million cells were injected into mast cell–deficient $kit^{W\text{-}sh/W\text{-}sh}$ mice via tail vein. Reconstituted mice were housed in pathogen-free circumstance for 16 wk and mast cell reconstitution in these recipients was histologically confirmed by toluidine blue staining of tissues from back skin before PSA experiments.

PCA. Experimental PCA was performed as previously described (Baba et al., 2008). Mice were injected intradermally with 1 μg (20 μl) IgE anti-DNP in the right ear and 20 μl saline in the left ear. The next day, the mice were challenged by intravenous injection of 100 μg DNP-BSA in 100 μl saline containing Evans blue dye (1%). Extravasation of Evans blue in the ear was monitored for 30 min, and ear biopsies were incubated at 63°C overnight in 700 μl formamide. Formamide extracts were analyzed by measuring the absorbance of Evans blue at 620 nm. Ear-swelling responses were assessed by measurement of ear thickness with a digital thickness gauge (G-1A). Net ear swelling was calculated as the difference in thickness of the right and left ears.

Airway inflammation. WT, Tespa1-deficient, mast cell–deficient ($Kit^{w\text{-}sh/w\text{-}sh}$) and $Kit^{w\text{-}sh/w\text{-}sh}$ mice that had been reconstituted with WT or Tespa1-deficient BMMCs were sensitized with OVA as previously described (Kopf et al., 2000; Williams and Galli, 2000; Izawa et al., 2012). Briefly, mice were intraperitoneally sensitized with 10 μg (100 μl) OVA (Sigma-Aldrich) on days 0, 7, 14, 21, 28, and 35. Then the mice were intranasally challenged with 20 μg (20 μl) OVA or PBS on days 40, 43, and 46. Mice were sacrificed 24 h after the last challenge. BALF was collected. Lung tissues were fixed with 10% formaldehyde and embedded in paraffin. Sections were stained with H&E and PAS (Williams and Galli, 2000; Xiao et al., 2011).

Immunoprecipitation and immunoblot analysis. Cells were lysed in NP-40 lysis buffer containing 50 mM Tris, pH 7.4, 150 mM NaCl, 1% NP-40, PMSF, and protease inhibitor cocktail (Sigma-Aldrich). The lysates were immunoprecipitated overnight at 4°C with the appropriate antibodies. Protein A/G Sepharose beads (Roche) were then added and the samples incubated for an additional 4–5 h. After washing three times, samples were resolved on SDS-PAGE gels (10%) and blotted. For immunoblot analysis, cells were lysed in SDS sample buffer by the addition of 1/4 volume of 5× SDS sample buffer directly into the cell suspensions. Samples were then boiled for 5 min and separated on 10% SDS-PAGE. Immunoblot analyses were done as described.

Ca^{2+} measurement. 1×10^7 BMMCs were suspended in 1 ml culture medium and sensitized with 1 µg/ml IgE anti-DNP for 6 h. Cells were washed twice with PBS and then loaded with 4 µM Fluo-4 AM (Molecular Probes) for 45 min. Cells were washed again and further incubated in PBS for 30 min at room temperature. 10 ng/ml DNP-BSA was then used to induce calcium flux, which was measured using a flow cytometer (FACSCalibur; BD) to monitor the fluorescent emission.

Immunofluorescence and confocal microscopy. Cells were fixed in prewarmed 4% paraformaldehyde for 15 min and permeabilized with 0.2% Triton X-100 for 5 min. After blocking with 5% BSA, cells were incubated overnight with anti-Tespa1 (1:50 in PBS containing 5% BSA), anti-Grb2, and anti-LAT2. Staining was detected using DyLight 488– and DyLight 549–labeled secondary antibody (Multiscience). Nuclei were co-stained with DAPI (Roche). Stained cells were viewed under a confocal fluorescence microscope (IX81-FV1000; Olympus).

FRET analysis and image processing. Cos7 cells plated on poly-L-lysine–coated glass-bottomed dishes (Matsunami Glass Ind. Ltd.) were imaged with an IX81-FV1000 confocal microscope equipped with three photomultipliers (PMTs), a heated-stage CO_2 chamber system, and an objective heater (Olympus) controlled by FV-10ASW software (Olympus). All imaging of living cells was done at 37°C. A water-immersion objective (LUMPlan FLN 60×; Olympus) was used exclusively for image acquisition. Alexa Fluor 546/647 FRET imaging was performed with sequential excitation at 543 nm and collection of donor–Alexa Fluor 546 (excitation, 555 nm; emission, 625 nm) and FRET (>650 nm) emission, followed by 633-nm excitation and acceptor–Alexa Fluor 647 (>650 nm) detection. Settings were kept unchanged for analysis of all samples. Unless otherwise indicated in the figure legends, donor emission was detected on PMT2, and acceptor and FRET emissions were recorded on PMT3. To determine donor and acceptor spectral bleed-throughs in the FRET setting, individual donor- or acceptor-stained samples were also imaged. After image acquisition, FRET images were calculated using FV-10ASW and ImageJ software (National Institutes of Health) with the plug-in program PixFRET. The calculated FRET efficiency (E) was as follows: $E = 1 - I^{DA}/I^{D}$, where I^{DA} indicates the fluorescence intensity of pre-bleach donor cells and I^{D} indicates the fluorescence intensity of post-bleach donor cells. $E > 0.05$ was defined as the threshold level for substantial transfer efficiency.

Flow cytometry for detection of Lat1 and Lat2. 2×10^5 BMMCs were spin-infected at 320 *g* for 90 min at 28°C with 200 µl lentivirus expressing Lat1 (SC-35796-V) or Lat2 (SC-62704-V)–specific shRNA or scrambled lentivirus (Santa Cruz Biotechnology, Inc.) in 10 µg/ml polybrene. Infected cells were cultured for 24 h, and then half of the medium was replaced with fresh medium containing cytokines. 48 h later, BMMCs were sensitized with anti-DNP IgE overnight and stimulated with 10 ng/ml DNP-BSA for calcium flux measurement. Or the cells were fixed with 100 µl IC fixation buffer (eBioscience), and then incubated in the dark at room temperature for 20 min. After two washes with 1× permeabilization buffer (eBioscience), cells were stained with LAT1 or LAT2 antibody at room temperature for 30 min. Cells were stained with APC-conjugated secondary antibody at room temperature for 30 min. Lat1 and Lat2 levels were measured using a flow cytometer (FACSCalibur; BD) to monitor the fluorescent emission.

Expression constructs and transient transfection of BMMCs. Thy1.1-Tespa1 constructs were transfected into BMMCs using mouse cell line Kit V (Amaxa) and the Nucleofector Device (program T-001; Amaxa). After transfection, cells were allowed to recover for 24 h in medium containing 10 ng/ml IL-3. Cells were then sensitized with anti–DNP-BSA overnight and stimulated with DNP-BSA for calcium flux measurement.

Statistical analyses. The unpaired Student's *t* test was used for analyses. P values <0.05 were considered statistically significant.

The authors thank Drs. Harvey Cantor (DFCI) and Hu Hu (ZJU) for helpful discussion; and Xinhui Song, Youfa Zhu, Shuangshuang Liu, and Yingying Huang from the core facilities (ZJU-SM) for technical assistance in histology and FACS analysis.

This work was supported by grants from the National Basic Research Program of China (973 Program; 2012CB945004 and 2011CB944100 to L. Lu) and the National Natural Science Foundation of China (31270927 and 31325009 to L. Lu, 31170842 and 31270927 to D. Wang). L. Lu also received funding support from the Specialized Research Fund for the Doctoral Program of Higher Education (20130101110004) and the Zhejiang University K.P. Chao High Technology Development Foundation.

The authors declare no competing financial interests.

Author contributions: D. Wang, M. Zheng, J. Wang, X. Cao, Y. Ke, Y.T. Zhou, and L. Lu designed the research; D. Wang, M. Zheng, Y. Qiu, C. Guo, J. Ji, L. Lei, X. Zhang, J. Liang, W. Huang, B. Dong, S. Wu, and J. Lou performed the research; D. Wang, M. Zheng, and L. Lu analyzed the data; D. Wang, M. Zheng, and L. Lu wrote the paper.

Submitted: 11 March 2014
Accepted: 4 November 2014

REFERENCES

Abassi, Y.A., J.A. Jackson, J. Zhu, J. O'Connell, X. Wang, and X. Xu. 2004. Label-free, real-time monitoring of IgE-mediated mast cell activation on microelectronic cell sensor arrays. *J. Immunol. Methods*. 292:195–205. http://dx.doi.org/10.1016/j.jim.2004.06.022

Alvarez-Errico, D., E. Lessmann, and J. Rivera. 2009. Adapters in the organization of mast cell signaling. *Immunol. Rev.* 232:195–217. http://dx.doi.org/10.1111/j.1600-065X.2009.00834.x

Baba, Y., K. Nishida, Y. Fujii, T. Hirano, M. Hikida, and T. Kurosaki. 2008. Essential function for the calcium sensor STIM1 in mast cell activation and anaphylactic responses. *Nat. Immunol.* 9:81–88. http://dx.doi.org/10.1038/ni1546

Bischoff, S.C. 2007. Role of mast cells in allergic and non-allergic immune responses: comparison of human and murine data. *Nat. Rev. Immunol.* 7:93–104. http://dx.doi.org/10.1038/nri2018

Brdicka, T., M. Imrich, P. Angelisová, N. Brdicková, O. Horváth, J. Spicka, I. Hilgert, P. Lusková, P. Dráber, P. Novák, et al. 2002. Non-T cell activation linker (NTAL): a transmembrane adaptor protein involved in immunoreceptor signaling. *J. Exp. Med.* 196:1617–1626. http://dx.doi.org/10.1084/jem.20021405

Brockmeyer, C., W. Paster, D. Pepper, C.P. Tan, D.C. Trudgian, S. McGowan, G. Fu, N.R. Gascoigne, O. Acuto, and M. Salek. 2011. T cell receptor (TCR)-induced tyrosine phosphorylation dynamics identifies THEMIS as a new TCR signalosome component. *J. Biol. Chem.* 286:7535–7547. http://dx.doi.org/10.1074/jbc.M110.201236

Fu, G., S. Vallée, V. Rybakin, M.V. McGuire, J. Ampudia, C. Brockmeyer, M. Salek, P.R. Fallen, J.A. Hoerter, A. Munshi, et al. 2009. Themis controls thymocyte selection through regulation of T cell antigen receptor-mediated signaling. *Nat. Immunol.* 10:848–856. http://dx.doi.org/10.1038/ni.1766

Fujimoto, T., H. Matsuzaki, M. Tanaka, and S. Shirasawa. 2013. Tespa1 protein is phosphorylated in response to store-operated calcium entry. *Biochem. Biophys. Res. Commun.* 434:162–165. http://dx.doi.org/10.1016/j.bbrc.2013.02.128

Galli, S.J., S. Nakae, and M. Tsai. 2005. Mast cells in the development of adaptive immune responses. *Nat. Immunol.* 6:135–142. http://dx.doi.org/10.1038/ni1158

Galli, S.J., M. Tsai, and A.M. Piliponsky. 2008. The development of allergic inflammation. *Nature*. 454:445–454. http://dx.doi.org/10.1038/nature07204

Garman, S.C., J.P. Kinet, and T.S. Jardetzky. 1999. The crystal structure of the human high-affinity IgE receptor (Fc epsilon RI alpha). *Annu. Rev. Immunol.* 17:973–976. http://dx.doi.org/10.1146/annurev.immunol.17.1.973

Gilfillan, A.M., and C. Tkaczyk. 2006. Integrated signalling pathways for mast-cell activation. *Nat. Rev. Immunol.* 6:218–230. http://dx.doi.org/10.1038/nri1782

Gu, H., K. Saito, L.D. Klaman, J. Shen, T. Fleming, Y. Wang, J.C. Pratt, G. Lin, B. Lim, J.P. Kinet, and B.G. Neel. 2001. Essential role for Gab2 in the allergic response. *Nature*. 412:186–190. http://dx.doi.org/10.1038/35084076

Izawa, K., Y. Yamanishi, A. Maehara, M. Takahashi, M. Isobe, S. Ito, A. Kaitani, T. Matsukawa, T. Matsuoka, F. Nakahara, et al. 2012. The receptor LMIR3 negatively regulates mast cell activation and allergic responses by binding to extracellular ceramide. *Immunity*. 37:827–839. http://dx.doi.org/10.1016/j.immuni.2012.08.018

Kalesnikoff, J., and S.J. Galli. 2008. New developments in mast cell biology. *Nat. Immunol.* 9:1215–1223. http://dx.doi.org/10.1038/ni.f.216

Kinet, J.P. 1999. The high-affinity IgE receptor (Fc epsilon RI): from physiology to pathology. *Annu. Rev. Immunol.* 17:931–972. http://dx.doi.org/10.1146/annurev.immunol.17.1.931

Kopf, M., A.J. Coyle, N. Schmitz, M. Barner, A. Oxenius, A. Gallimore, J.C. Gutierrez-Ramos, and M.F. Bachmann. 2000. Inducible costimulator protein (ICOS) controls T helper cell subset polarization after virus and parasite infection. *J. Exp. Med.* 192:53–62. http://dx.doi.org/10.1084/jem.192.1.53

Kraft, S., and J.P. Kinet. 2007. New developments in FcepsilonRI regulation, function and inhibition. *Nat. Rev. Immunol.* 7:365–378. http://dx.doi.org/10.1038/nri2072

Matsuzaki, H., T. Fujimoto, M. Tanaka, and S. Shirasawa. 2013. Tespa1 is a novel component of mitochondria-associated endoplasmic reticulum membranes and affects mitochondrial calcium flux. *Biochem. Biophys. Res. Commun.* 433:322–326. http://dx.doi.org/10.1016/j.bbrc.2013.02.099

McPherson, V.A., S. Everingham, R. Karisch, J.A. Smith, C.M. Udell, J. Zheng, Z. Jia, and A.W. Craig. 2009. Contributions of F-BAR and SH2 domains of Fes protein tyrosine kinase for coupling to the FcεRI pathway in mast cells. *Mol. Cell. Biol.* 29:389–401. http://dx.doi.org/10.1128/MCB.00904-08

Metcalfe, D.D., D. Baram, and Y.A. Mekori. 1997. Mast cells. *Physiol. Rev.* 77:1033–1079.

Orr, S.J., and D.W. McVicar. 2011. LAB/NTAL/Lat2: a force to be reckoned with in all leukocytes? *J. Leukoc. Biol.* 89:11–19. http://dx.doi.org/10.1189/jlb.0410221

Paster, W., C. Brockmeyer, G. Fu, P.C. Simister, B. de Wet, A. Martinez-Riaño, J.A. Hoerter, S.M. Feller, C. Wülfing, N.R. Gascoigne, and O. Acuto. 2013. GRB2-mediated recruitment of THEMIS to LAT is essential for thymocyte development. *J. Immunol.* 190:3749–3756. http://dx.doi.org/10.4049/jimmunol.1203389

Rivera, J. 2005. NTAL/LAB and LAT: a balancing act in mast-cell activation and function. *Trends Immunol.* 26:119–122. http://dx.doi.org/10.1016/j.it.2005.01.001

Rivera, J., and A.M. Gilfillan. 2006. Molecular regulation of mast cell activation. *J. Allergy Clin. Immunol.* 117:1214–1225, quiz:1226. http://dx.doi.org/10.1016/j.jaci.2006.04.015

Saitoh, S., S. Odom, G. Gomez, C.L. Sommers, H.A. Young, J. Rivera, and L.E. Samelson. 2003. The four distal tyrosines are required for LAT-dependent signaling in FcεRI-mediated mast cell activation. *J. Exp. Med.* 198:831–843. http://dx.doi.org/10.1084/jem.20030574

Siraganian, R.P. 2003. Mast cell signal transduction from the high-affinity IgE receptor. *Curr. Opin. Immunol.* 15:639–646. http://dx.doi.org/10.1016/j.coi.2003.09.010

Su, A.I., T. Wiltshire, S. Batalov, H. Lapp, K.A. Ching, D. Block, J. Zhang, R. Soden, M. Hayakawa, G. Kreiman, et al. 2004. A gene atlas of the mouse and human protein-encoding transcriptomes. *Proc. Natl. Acad. Sci. USA*. 101:6062–6067. http://dx.doi.org/10.1073/pnas.0400782101

Suzuki, R., S. Leach, W. Liu, E. Ralston, J. Scheffel, W. Zhang, C.A. Lowell, and J. Rivera. 2014. Molecular editing of cellular responses by the high-affinity receptor for IgE. *Science*. 343:1021–1025. http://dx.doi.org/10.1126/science.1246976

Teramoto, H., P. Salem, K.C. Robbins, X.R. Bustelo, and J.S. Gutkind. 1997. Tyrosine phosphorylation of the vav proto-oncogene product links FcεRI to the Rac1-JNK pathway. *J. Biol. Chem.* 272:10751–10755. http://dx.doi.org/10.1074/jbc.272.16.10751

Vennekens, R., J. Olausson, M. Meissner, W. Bloch, I. Mathar, S.E. Philipp, F. Schmitz, P. Weissgerber, B. Nilius, V. Flockerzi, and M. Freichel. 2007. Increased IgE-dependent mast cell activation and anaphylactic responses in mice lacking the calcium-activated nonselective cation channel TRPM4. *Nat. Immunol.* 8:312–320. http://dx.doi.org/10.1038/ni1441

Volná, P., P. Lebduska, L. Dráberová, S. Símová, P. Heneberg, M. Boubelík, V. Bugajev, B. Malissen, B.S. Wilson, V. Horejsí, et al. 2004. Negative regulation of mast cell signaling and function by the adaptor LAB/NTAL. *J. Exp. Med.* 200:1001–1013. http://dx.doi.org/10.1084/jem.20041213

Wang, D., M. Zheng, L. Lei, J. Ji, Y. Yao, Y. Qiu, L. Ma, J. Lou, C. Ouyang, X. Zhang, et al. 2012. Tespa1 is involved in late thymocyte development through the regulation of TCR-mediated signaling. *Nat. Immunol.* 13:560–568. http://dx.doi.org/10.1038/ni.2301

Williams, C.M., and S.J. Galli. 2000. Mast cells can amplify airway reactivity and features of chronic inflammation in an asthma model in mice. *J. Exp. Med.* 192:455–462. http://dx.doi.org/10.1084/jem.192.3.455

Xiao, W., J. Kashiwakura, H. Hong, H. Yasudo, T. Ando, M. Maeda-Yamamoto, D. Wu, Y. Kawakami, and T. Kawakami. 2011. Phospholipase C-β3 regulates FcεRI-mediated mast cell activation by recruiting the protein phosphatase SHP-1. *Immunity*. 34:893–904. http://dx.doi.org/10.1016/j.immuni.2011.04.010

Zhu, M., Y. Liu, S. Koonpaew, O. Granillo, and W. Zhang. 2004. Positive and negative regulation of FcεRI-mediated signaling by the adaptor protein LAB/NTAL. *J. Exp. Med.* 200:991–1000. http://dx.doi.org/10.1084/jem.20041223